



LAWRENCE
LIVERMORE
NATIONAL
LABORATORY

Computational Design of Short Pulse Laser Driven Iron Opacity Measurements

M. E. Martin

June 15, 2015

2015 ANS Winter Meeting and Nuclear Technology Expo
Washington, DC, United States
November 8, 2015 through November 12, 2015

Disclaimer

This document was prepared as an account of work sponsored by an agency of the United States government. Neither the United States government nor Lawrence Livermore National Security, LLC, nor any of their employees makes any warranty, expressed or implied, or assumes any legal liability or responsibility for the accuracy, completeness, or usefulness of any information, apparatus, product, or process disclosed, or represents that its use would not infringe privately owned rights. Reference herein to any specific commercial product, process, or service by trade name, trademark, manufacturer, or otherwise does not necessarily constitute or imply its endorsement, recommendation, or favoring by the United States government or Lawrence Livermore National Security, LLC. The views and opinions of authors expressed herein do not necessarily state or reflect those of the United States government or Lawrence Livermore National Security, LLC, and shall not be used for advertising or product endorsement purposes.

Computational Design of Short Pulse Laser Driven Iron Opacity Measurements

Madison E. Martin,^{*,†} Richard London,[†] Sedat Goluoglu,^{*} and Heather Whitley[†]

[†]*Lawrence Livermore National Laboratory, 7000 East Ave., Livermore, CA*

^{*}*University of Florida, Gainesville, FL*

martin240@llnl.gov

INTRODUCTION

Radiation plays an important role in the energy transfer of high energy density (HED) systems such as stars and inertial confinement fusion (ICF) implosions. Radiation transport is a multi-step process which includes photon emission by matter, transport in matter, and interaction with matter (either by absorption or scattering). Optically thick systems, such as star and ICF implosions, have many interactions within the plasma leading to less efficient radiation transfer. In stars, energy generated by fusion in the core is transported from the center to the stellar surface through both radiative and convective heat transfer. The opacity of the ICF target materials play a large role in the efficiency of energy transport during the target implosion.

Both ICF and stellar physics require the use of computational models to understand energy transport. ICF targets and laser pulses are designed through the use of radiation hydrodynamic codes. Solar models are mathematical representations of the sun, most often treated as a spherically symmetric plasma, that rely on energy transport models. Typically, numerical methods to solve the radiation transport equation incorporate opacity in either theoretically based formulas or tables that characterize the atomic structure and transitions for each element in the system's plasma. Statistical methods are required for elements with a large number of ionization stages, making the models more complex and less certain. Experimental validation of opacity for such elements and conditions are particularly important. It is impractical to test every set of conditions and elements used in theoretical opacity models due to the volume of data and degrees of freedom in the problem. Therefore, opacity measurements for a subset of plasma conditions are desired to test and validate the physical assumptions used in opacity models. Hence, if the model can be validated experimentally, extrapolation to other conditions and elements may be justified.

The resolution of current disagreements between solar models and helioseismological observations would benefit from experimental validation of theoretical opacity models for materials such as carbon, nitrogen, oxygen, and iron [1, 2]. Specifically, experimental opacity measurements for electron temperatures greater than 100 eV and densities larger than a fraction of solid density are needed in order to investigate the uncertainties in theoretical opacity models for stellar relevant materials [3]. In a recent *Nature* paper, Bailey et al. performed a thorough comparison of pulsed power driven iron opacity measurements (temperatures of 160-200 eV and densities of 10^{-3} to 10^{-2} of solid density, comparable to the base of the convective zone of the sun) to a variety of different opacity models [4]. They concluded that the measured opacity is 30 to 400 % larger than predicted values. This suggests there

may be some physical concepts not incorporated into the existing opacity models or the approximations used to speed up computational efficiency do not provide enough detail for this regime. Bailey et al. also suggest that the increased opacity accounts for $\approx 50\%$ of the discrepancy between calculated solar parameters using the revised lower element abundances and helioseismological observations.

Short pulse laser driven opacity experiments can reach temperatures of 200-400 eV and densities of 10^{-1} to solid density, similar to the radiative zone of the sun. Computational experimental design must be done to optimize the target characteristics and laser conditions such that specific plasma conditions and emission spectrum are achieved. The radiation hydrodynamics code HYDRA [5] was used to investigate the effect of increasing laser irradiance on the plasma conditions and emission of an iron buried layer opacity target. Measurements of this nature would investigate the validity of existing theoretical opacity models and may possibly resolve some of the discrepancy between solar parameters calculated from solar models using the revised lower element abundances and helioseismological observations.

THEORY

Radiation transfer is generally modeled by a differential equation for the radiation intensity (Eq. (1)). This radiation transfer equation includes terms for the temporal and spatial change in radiation intensity as well as terms representing the emission and loss of radiation.

$$\begin{aligned} \frac{1}{c} \frac{\partial}{\partial t} (I_\nu(\mathbf{r}, t; \boldsymbol{\Omega}, h\nu)) + \frac{\partial}{\partial s} (I_\nu(\mathbf{r}, t; \boldsymbol{\Omega}, h\nu)) \\ = \eta_\nu(\mathbf{r}, t; \boldsymbol{\Omega}, h\nu) - \chi_\nu(\mathbf{r}, t; \boldsymbol{\Omega}, h\nu) I_\nu(\mathbf{r}, t; \boldsymbol{\Omega}, h\nu) \end{aligned} \quad (1)$$

The specific intensity, $I_\nu(\mathbf{r}, t; \boldsymbol{\Omega}, h\nu)$, represents the radiant energy per units of time, solid angle, area, and photon energy moving in direction \mathbf{r} . The emissivity, $\eta_\nu(\mathbf{r}, t; \boldsymbol{\Omega}, h\nu)$, represents the emitted energy. The opacity coefficient, $\chi_\nu(\mathbf{r}, t; \boldsymbol{\Omega}, h\nu)$, represents the absorption per unit length.

Short pulse laser driven opacity experiments using buried layer targets can be used to infer the opacity of the target material. As seen in Figure 1, the material of interest is tamped by a low-Z material. The short pulse laser irradiates one side of the tamper, creating hot electrons at the surface of the target which transport through and heat the target. The heated target emits x-rays which are recorded by a spectrometer.

For this configuration, Eq. (1) can be solved assuming steady state, 1D-planar geometry with constant properties to get

$$I_\nu = \frac{\eta_\nu}{\kappa_\nu} (1 - e^{-\kappa_\nu \rho \Delta t}), \quad (2)$$

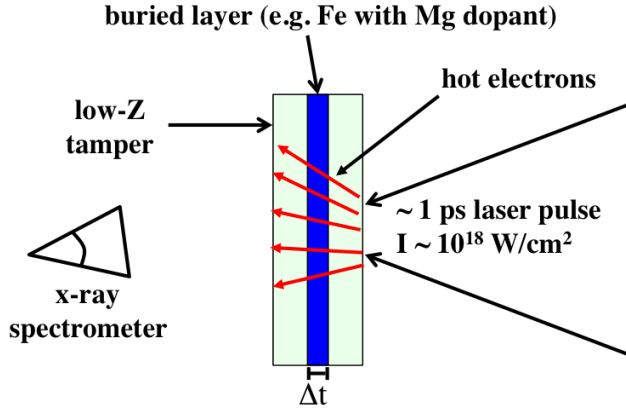


Fig. 1. Schematic of a short pulse laser driven opacity measurement [6].

where κ_v is the opacity in cm^2/g , ρ is the plasma density in g/cm^3 , and Δt is the thickness of the buried layer.

With emission spectroscopy experiments, local thermodynamic equilibrium (LTE) must be assumed so that opacity can be inferred from the emission spectra. Presuming LTE allows for the source term to be replaced by the Planckian function $B_v(T)$,

$$B_v(T) = \frac{\eta_v}{\kappa_v}. \quad (3)$$

Using Eq. (2) and Eq. (3), the opacity can be calculated by

$$\kappa_v = \frac{-\ln\left(1 - \frac{I_v}{B_v(T)}\right)}{\rho \Delta t} \quad (4)$$

where the specific intensity I_v is measured by a spectrometer. In addition to measuring the target's spectral emission, a dopant material is needed in the buried layer so that the plasma temperature and density can be inferred. Ideally, a dopant material would have K-shell ions at the temperature of the experiment, so that there are only two ionic transitions to calculate, making detailed atomic modeling simple. The plasma temperature can be inferred by comparing the ratio of different atomic transition lines which determine the ionization potential and thus the temperature. The plasma density can be inferred by analyzing the stark broadened line widths which indicate density.

COMPUTATIONAL DESIGN

Computational design is needed to optimize target dimensions, dopant material for temperature/density measurements, and incident laser pulses. The intensity of the target emission spectrum is simulated and optimized to produce signals that can be accurately measured. HYDRA has been used to analyze the effect of changing laser irradiance on the plasma temperature, plasma density, and target emission. The goal of this parameter study is to investigate the laser irradiance required to design iron opacity measurements at temperatures of 200 to 400eV and densities of 10^{-1} to solid density.

The HYDRA models reported here assume 1D geometry, use multigroup diffusion for radiation transport and use detailed configuration accounting (DCA) model [7, 8] for atomic structure and opacity. An incremental internal energy source is specified for a Gaussian power pulse that mimics the laser pulse. The maximum internal energy is selected to mimic the average laser energy per unit mass, which is related to the laser irradiance. The Gaussian power pulse is constructed to have the same full width half max (FWHM) as the laser pulse and total integrated value equal to the deposited energy previously described.

In order to mimic modifying the laser irradiance, a series of models were created by varying the energy deposition such that it is consistent with laser irradiances of $1.0 \times 10^{17} \text{ W}/\text{cm}^2$ to $2.0 \times 10^{18} \text{ W}/\text{cm}^2$ (FWHM = 1ps for all models). The target consisted of a $5 \mu\text{m}$ tamper of parylene-N on either side of a $0.2 \mu\text{m}$ layer of iron. For all models, 5 % of the laser energy is deposited in the entire target. This percentage is selected to account for the conversion of absorbed laser light to hot electrons and the coupling of hot electrons to energy deposition in the target. In this way, the energy deposition represents the heating of the target by hot electrons generated by absorbed laser light. The target dimensions and materials remained constant for all models. While the parameter study included more models, only four models will be used in this analysis. The $1.0 \times 10^{17} \text{ W}/\text{cm}^2$ and $2.0 \times 10^{18} \text{ W}/\text{cm}^2$ models are selected to indicate the extremes of the parameter study. The $6.0 \times 10^{17} \text{ W}/\text{cm}^2$ and $1.1 \times 10^{18} \text{ W}/\text{cm}^2$ are selected to demonstrate that peak electron temperatures and densities consistent with the radiative zone of the sun, 200 to 400eV and densities of 10^{-1} to solid density, can be achieved.

RESULTS AND ANALYSIS

Yorick [9], an interpreted language for scientific simulations and calculations, is used to analyze each model's electron temperature, material density, and x-ray emission. The x-ray emission is simulated by a Yorick function that solves the radiation transport equation in each zone along a user specified ray that intersects the model's spatial grid. The function uses the zonal opacity and emissivity values from the HYDRA model being analyzed.

The general behavior of a buried layer model can be seen in Figure 2, where the rapid heating of the target around 2 ps results in a quick increase in electron temperature. The rapid heating correlates with the expansion of the buried layer, which can be seen by the widening of buried layer boundaries and the drop in material density. At around 7 ps, the buried layer is compressed by the expansion of the tamper into the iron layer. Later in time the buried layer expands again. This general behavior is seen in all HYDRA models analyzed.

The average electron temperature in the iron layer is compared for four models in Figure 3. It is seen that as energy deposition is increased, the average temperature in the iron layer increases. This is true for all times, but is most evident at the time of peak temperature.

In Figure 4, the rapid drop in iron layer's average density at early time indicates the rapid expansion of the buried layer while it is heated. The increase in average density represents

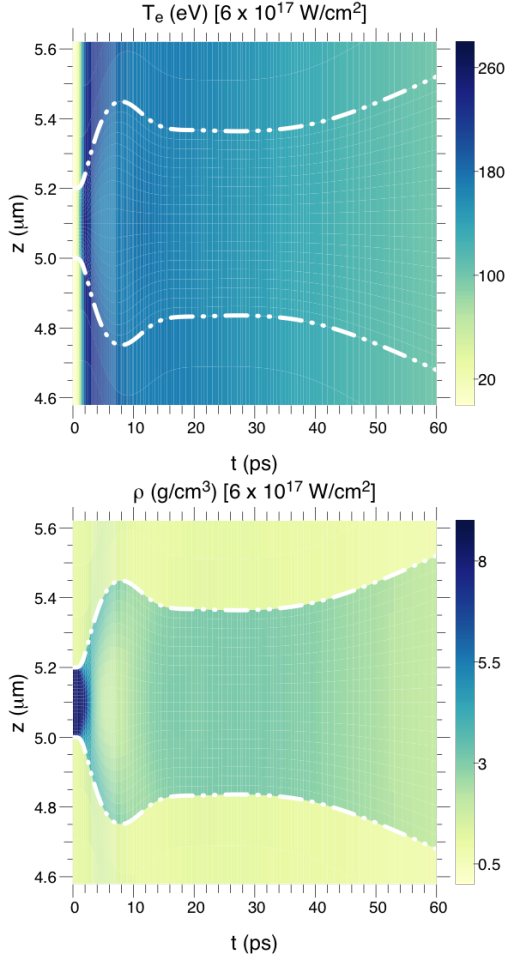


Fig. 2. Typical behavior of electron temperature and material density with respect to time and position. The white dash-dot-dot lines represent the iron buried layer boundaries. These plots for the model consistent with $6 \times 10^{17} \text{ W/cm}^2$.

compression as the tamper expands into the buried layer. As energy deposition is increased, the rate of the initial expansion and the rate of the compression of the buried layer increase. In addition, the minimum average density decreases with increasing energy deposition. In general, the average density quickly drops followed by an increase and a period of constant density before ultimately decreasing. The length of time for which the average density is approximately constant decreases as energy deposition increases.

Figure 5, shows the simulated x-ray emission and inferred opacity at time of peak temperature for the spectral range of interest (0.7 - 1.7 keV). The inferred opacity is calculated using Eq. (4). The specific intensity for the $1.0 \times 10^{17} \text{ W/cm}^2$ model is orders of magnitude smaller than the specific intensities of the other models. As energy deposition is increased, the specific intensity of the x-ray emission increases. In addition, the average ionization increases resulting in a shift in emission to higher energy ranges.

The inferred opacity shows both similarities and differences from the specific intensity. Even though the $1.0 \times$

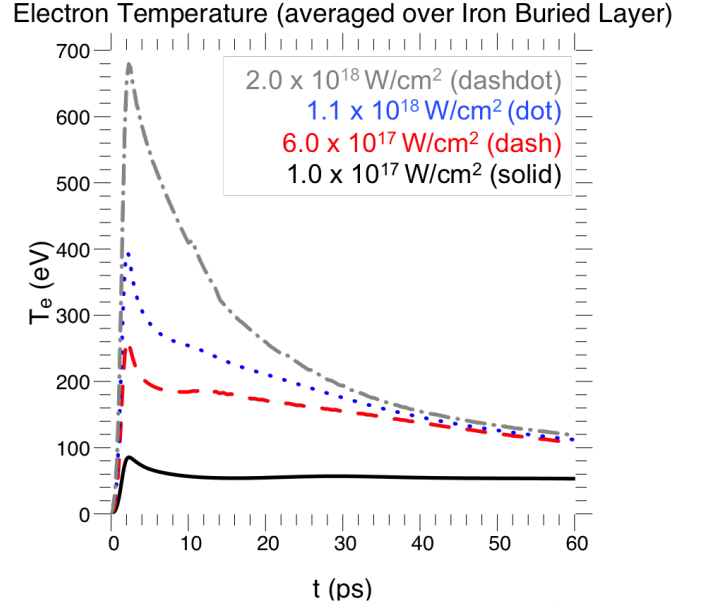


Fig. 3. As the energy deposition is increased the average electron temperature of the iron layer increases.

10^{17} W/cm^2 emission is small compared to the other models, the inferred opacity has values that are a fraction of the other models' inferred opacity. However, the inferred opacity for the $1.0 \times 10^{17} \text{ W/cm}^2$ model has no line features in this spectral range and is dominated by the continuum emission of the target. This is because the iron buried layer is not sufficiently heated to cause the atomic transitions of interest in this spectral range.

Based on this energy deposition study, a laser irradiance of $\approx 1 \times 10^{17} \text{ W/cm}^2$ would not be sufficient to reach the plasma conditions or emission similar to the radiative zone of the sun. In order to reach temperatures of 200 to 400 eV, densities of 10^{-1} to solid density, and sufficient x-ray emission, a laser irradiance of $\approx 6 \times 10^{17} \text{ W/cm}^2$ to $1 \times 10^{18} \text{ W/cm}^2$ is required.

CONCLUSIONS

The energy deposition design study showed that a $\approx 1 \times 10^{18} \text{ W/cm}^2$ laser pulse incident on iron buried layer target can reach electron temperatures of $\approx 400 \text{ eV}$ and densities near the solid value, which are consistent with temperatures and densities of the radiative zone of the sun. The electron temperature and overall x-ray emission signal can be increased by increasing the laser irradiance. Experiments such as these will examine the validity of theoretical opacity models at these regimes. The physical understanding gained can be applied to other materials at similar temperatures and densities. These high energy density regimes are important to not only stellar physics, but also inertial confinement fusion implosions. In addition, knowledge gained from this type of experimental investigation will serve to validate and/or help inform future opacity calculations.

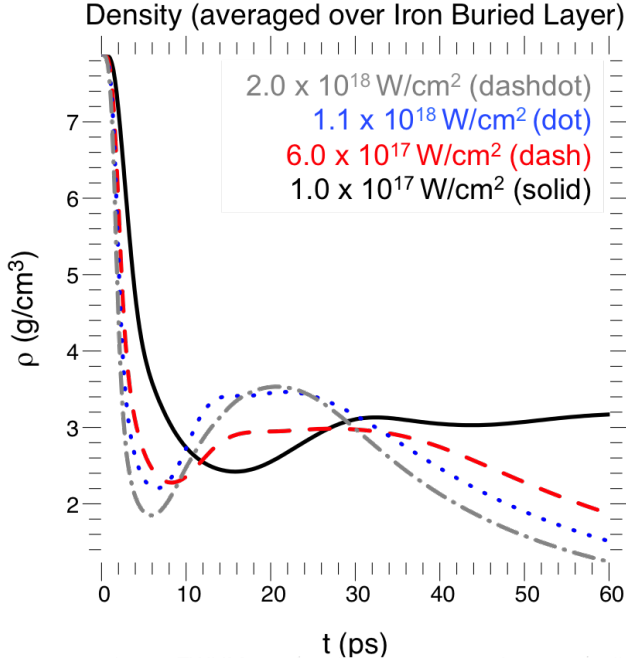


Fig. 4. As the energy deposition is increased, the rate of initial expansion of the buried layer increases which can be seen as an increase in the slope of the initial density drop.

ACKNOWLEDGMENTS

This work was performed under the auspices of the U.S. Department of Energy by Lawrence Livermore National Laboratory under Contract DE-AC52-07NA27344. Lawrence Livermore National Security, LLC. LLNL-CONF-673217

REFERENCES

1. J. N. BAHCALL and ET AL., "Helioseismological Implications of Recent Solar Abundance Determinations," *The Astrophysical Journal*, **618**, 1049 (January 2005).
2. S. BASU and H. M. ANITA, "Helioseismology and solar abundances," *Physics Reports*, **457**, 217 (December 2008).
3. S. TURCK-CHIÈZE and ET AL., "On plasma radiative properties in stellar conditions," *High Energy Density Physics*, **5**, 132 (2009).
4. J. E. BAILEY and ET AL., "A higher-than-predicted measurement of iron opacity at solar interior temperatures," *Nature*, **517**, 56 (2015).
5. M. M. MARINAK and ET AL., "Three-dimensional HYDRA simulations of National Ignition Facility targets," *Physics of Plasmas*, **8**, 5, 2275 (May 2001).
6. R. LONDON and J. CASTOR, "Design of short pulse laser driven opacity experiments," *High Energy Density Physics*, **9**, 725 (2013).
7. Y. T. LEE, "A model for ionization balance and L-shell spectroscopy of non-LTE plasmas," *Journal of Quantitative Spectroscopy and Radiative Transfer*, **38**, 2, 131 (1987).
8. H. A. SCOTT and S. B. HANSEN, "Advances in NLTE modeling for integrated simulations," *High Energy Density*

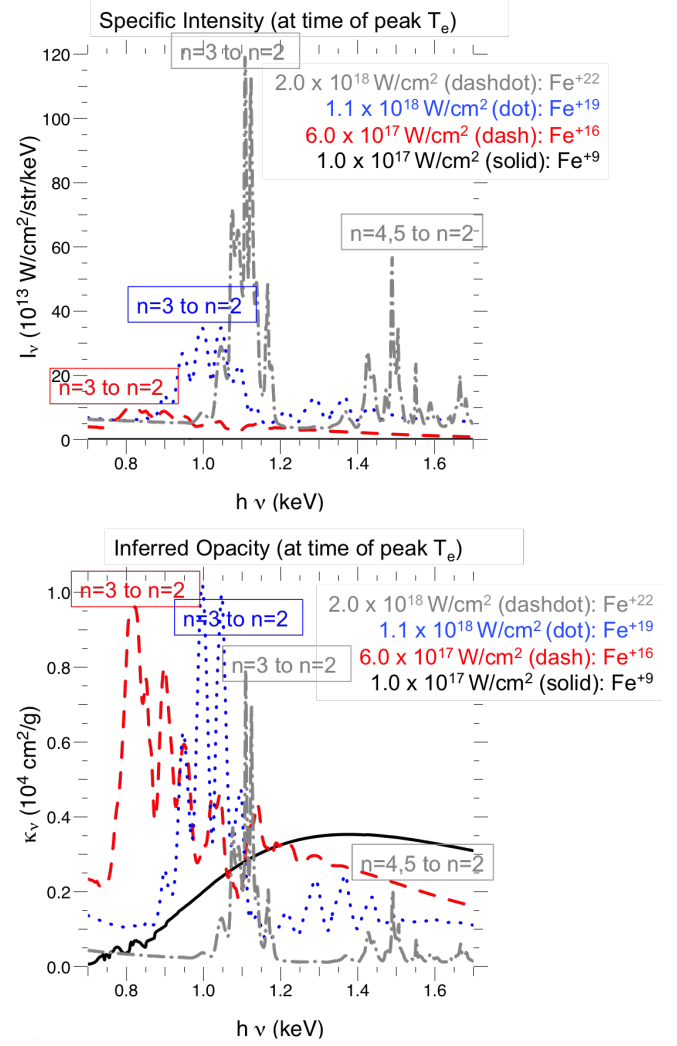


Fig. 5. Simulated x-ray emission and inferred opacity for the four models. The boxed notation is the atomic transition represented by that range of spectral energies. The upper right of each plot includes the average ionization of the iron buried layer at the time of peak temperature for each model.

Physics, **6**, 39 (2010).

9. D. MUNRO, <http://yorick.sourceforge.net/>.